Solar Physics
DOI: 10.1007/•••••-•••-•••-••••-•

Formation of Radio Type II Bursts During a Multiple Coronal Mass Ejection Event

Firas Al-Hamadani [1,2] · **Silja Pohjolainen**[3,1] · **Eino Valtonen** [1]

Abstract We study a solar event on 27 September 2001 that consisted of three consecutive coronal mass ejections (CMEs) originating from the same active region, and which were associated with several periods of radio type II burst emission at decameter-hectometer (DH) wavelengths. Our analysis shows that the first radio burst originated from a low-density environment, formed in the wake of the first, slow CME. The frequency-drift of the burst suggests a low-speed burst driver, or that the shock was not propagating along the large density gradient. There is also evidence of band-splitting within this emission lane. The origin of the first shock remains unclear, as several alternative scenarios exist. The second shock showed separate periods of enhanced radio emission. This shock could have originated from a CME bow shock, caused by the fast and accelerating second or third CME. However, a shock at CME flanks is also possible, as the density depletion caused by the three CMEs would have affected the emission frequencies and hence the radio source heights could have been lower than usual. The last type II burst period showed enhanced emission in a wider bandwidth, which was most probably due to the CME – CME interaction. Only one shock that could reliably be associated with the investigated CMEs was observed to arrive near Earth.

Keywords: Coronal Mass Ejections, Initiation and Propagation, Radio Bursts, Meter-Wavelengths and Longer (m, dkm, hm, km), Type II

✉ F. Al-Hamadani
fimubaa@utu.fi

S. Pohjolainen
silpoh@utu.fi

E. Valtonen
eino.valtonen@utu.fi

[1] Department of Physics and Astronomy, University of Turku, Turku, Finland

[2] Department of Physics, University of Basrah, Basrah, Iraq

[3] Tuorla Observatory, University of Turku, Piikkiö, Finland

1. Introduction

Our understanding about the physical phenomena of the solar corona and interplanetary (IP) medium can be enhanced by studying radio type II bursts that are known to be caused by propagating shock waves (*e.g.* Cane and Erickson, 2005). Electrons accelerated by the shock produce Langmuir waves in the surrounding plasma, and these eventually turn into radio waves. Type II bursts are frequency-drifting emissions, where the drift rates reflect the decreasing density in the solar atmosphere as the plasma frequency changes as $f_{\rm p} = 9000\sqrt{n_e}$ ($f_{\rm p}$ in Hz and electron density n_e in cm^{-3}). Type II bursts are often identified with fundamental and harmonic plasma emission bands, although at decameter-hectometer (DH) wavelengths the harmonic band can be undetectable due to plasma processes (see Pohjolainen, Allawi, and Valtonen, 2013, and references therein). Sometimes the emission is also band-split. Band-splitting is frequently considered to be a consequence of plasma emission from upstream and downstream shock regions (Smerd, Sheridan, and Stewart, 1974, 1975). Other explanations for the band-split include coronal density gradients and causes inherent in the emission process itself (*e.g.* Treumann and Labelle, 1992). Gaps in the radio emission lanes which are sometimes observed can be explained if the shock propagates through low-density regions where the Alfvén speed rises temporarily (Knock and Cairns, 2005).

The relationship between type II bursts at meter and DH wavelengths, and their association with flares and coronal mass ejections (CMEs), have been investigated by various authors (*e.g.* Gosling, 1993; Dryer, 1996; Shanmugaraju *et al.*, 2003). For example, there have been arguments on the association and relative timing of type II bursts with CMEs and flares (*e.g.* Gopalswamy *et al.*, 1998; Cliver, Webb, and Howard, 1999). A statistical study by Prakash *et al.* (2009) found that most of the coronal (meter wave) shocks dissolve before they arrive to IP space. However, it is now generally accepted that the observed DH type II radio bursts are caused by CME-driven shock waves (*e.g.* Lara *et al.*, 2003; Gopalswamy *et al.*, 2005; Cho *et al.*, 2005).

Radio signatures produced by interacting CMEs were first reported by Gopalswamy *et al.* (2001, 2002). A case study performed by Maričić *et al.* (2014) found that the velocity of the earlier CME increased after the interaction, while the velocity of the later CME decreased.

In this article we analyse radio emission that was associated with three successive CMEs, launched from the same active region within a short period of time on 27 September 2001. The CMEs were associated with low-intensity solar flares and strong type II radio emission at DH wavelengths. The aim of this study is to analyse the radio emission and its association with the CMEs, and to discuss the role of CME interaction during the propagation of different CME structures.

2. Data Analysis

The event on 27 September 2001 was selected for analysis because it presented clear periods of type II burst emission that could be associated with the prop-

agation of multiple (but separable) CMEs. Furthermore, the first type II burst showed features that could not easily be associated with any particular CME and therefore deserved a closer study.

The *Solar and Heliospheric Observatory* (SOHO)/*Large Angle and Spectrometric Coronagraph* (LASCO) (Brueckner *et al.*, 1995) observations and the LASCO CME catalog were used for deriving the CME characteristics. The data for the IP radio type II events were taken from the *Wind*/WAVES (Bougeret *et al.*, 1995) catalogue, prepared by Michael L. Kaiser. The flare data are available from the National Oceanic and Atmospheric Administration (NOAA) listings. Solar X-ray fluxes were measured by the *Geostationary Operational Environmental Satellite* (GOES), and X-ray imaging was provided by the *Yohkoh Soft X-ray Telescope* (SXT: Tsuneta *et al.*, 1991). The SOHO/*Extreme-Ultraviolet Imaging Telescope* (EIT: Delaboudinière *et al.*, 1995) images were used to investigate structures in EUV. Hα images came from the Kanzelhöhe Solar Observatory, provided by the Global High Resolution Hα Network.

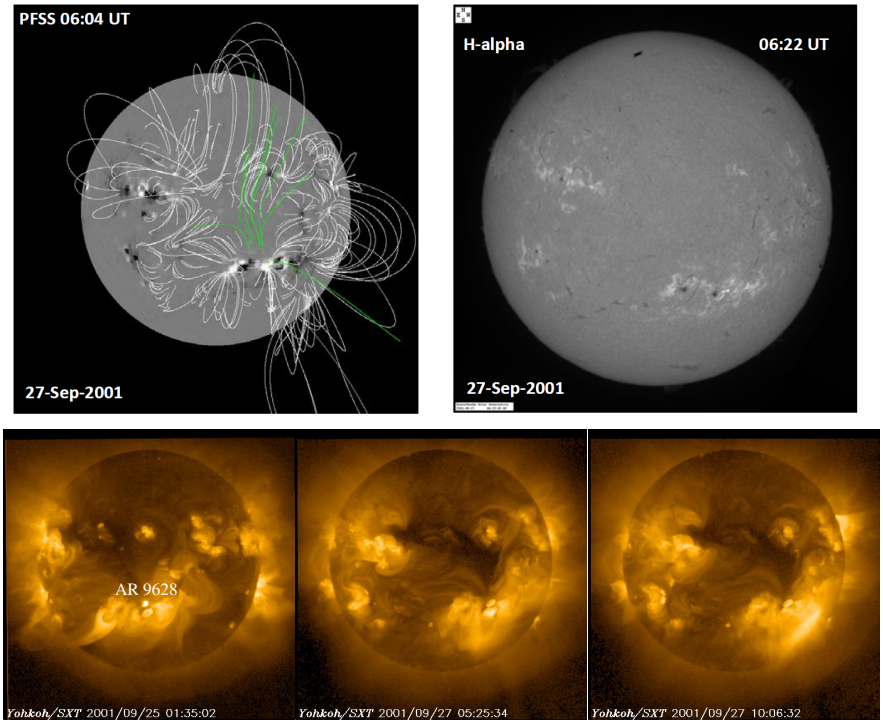

Figure 1. Potential magnetic field at 06:04 UT plotted with the Solarsoft PFSS program (top left), Kanzelhöhe Hα image at 06:22 UT (top right). The bottom panel shows *Yohkoh*/SXT full-disk images at 01:35 UT on 25 September 2001 and at 05:25 UT and 10:06 UT on 27 September 2001. The images are from the LASCO CME Catalog .

2.1. Active Region Characteristics and Flares

The complex NOAA active region (AR) 9628 had Beta-Gamma-Delta magnetic classification, which predicts high probability of flaring. Several small Hα flares

Table 1. CME and flare characteristics of the solar events in NOAA AR 9628, observed on 26 – 27 September 2001. The CME speeds were estimated from second order fits to the CME fronts, observed in projection.

Event	First C2 appearance (UT)	Speed near 4 $R_\odot$ (km s^{-1})	Speed near 20 $R_\odot$ (km s^{-1})	Hα flare start (UT)	Flare class (GOES)	Flare location
CME1	01:32	190	–	23:07[1]	C[2]	S20W23
CME1 core	01:32	140	780	–	–	–
CME2	04:54	280	–	04:24	C3.8	S20W27
CME2 core	05:30	140	750	–	–	–
CME3	08:06	500	800	07:51	C[3]/M1.0	S18W39

[1]Closest-in-time flare in the same AR, on 26 September 2001.
[2]X-ray enhancement but no GOES classification, association unknown.
[3]Flare impulsive start C-class, peak of later long-duration emission M1.0.

were reported in this active region during the time period 26 September 23:07 UT – 27 September 08:23 UT. The reported flare locations were in the range S20W23 – S18W39. These flares had very small X-ray intensities measured by GOES, and for some no association could be established between the X-ray and Hα emission. The enhancements observed by GOES were all C-class, except the last flare which was associated with a long-duration X-ray enhancement that eventually reached GOES class M1.0 at 12:13 UT. The Hα image at 06:22 UT in Figure 1 shows one of the small flares located at S19W28. The flares that occurred during or before the lift-off phase of the analysed CMEs are listed in Table 1.

The potential magnetic field of this region, plotted with the PFSS software and shown in Figure 1, consists of large-scale loops connected to nearby active regions, as well as open magnetic field lines (plotted green in the image).

The *Yohkoh*/SXT full-disk image (Figure 1) shows AR 9628 near disk centre on 25 September 2001. The large-scale loops connect the AR to smaller active regions in the northern hemisphere, but no other active regions are visible in the south-west. On 27 September 2001 the largest loops in AR 9628 are located near the south-western solar limb (Figure 1), and the closeness to the limb may have caused the difficulties in associating the Hα and X-ray flares, as most of the heated X-ray plasma appeared above the limb.

No large-scale waves or dimming phenomena were observed during these events; see the SOHO EIT difference images at 08:24 and 08:48 UT in Figure 2. This suggests that no shock waves were formed in the chromosphere or in the low corona, and that the ejected material within the CMEs was most probably plasma loops and filaments. It is possible that this CME was of the type described by Robbrecht, Patsourakos, and Vourlidas (2009), initiated by the lift-off of a flux-rope from an unusually large height. In cases where we do not see on-the-disk signatures, it is also possible that the CME was a back-side event. In the present case no other active regions were observed nearby on earlier dates, that

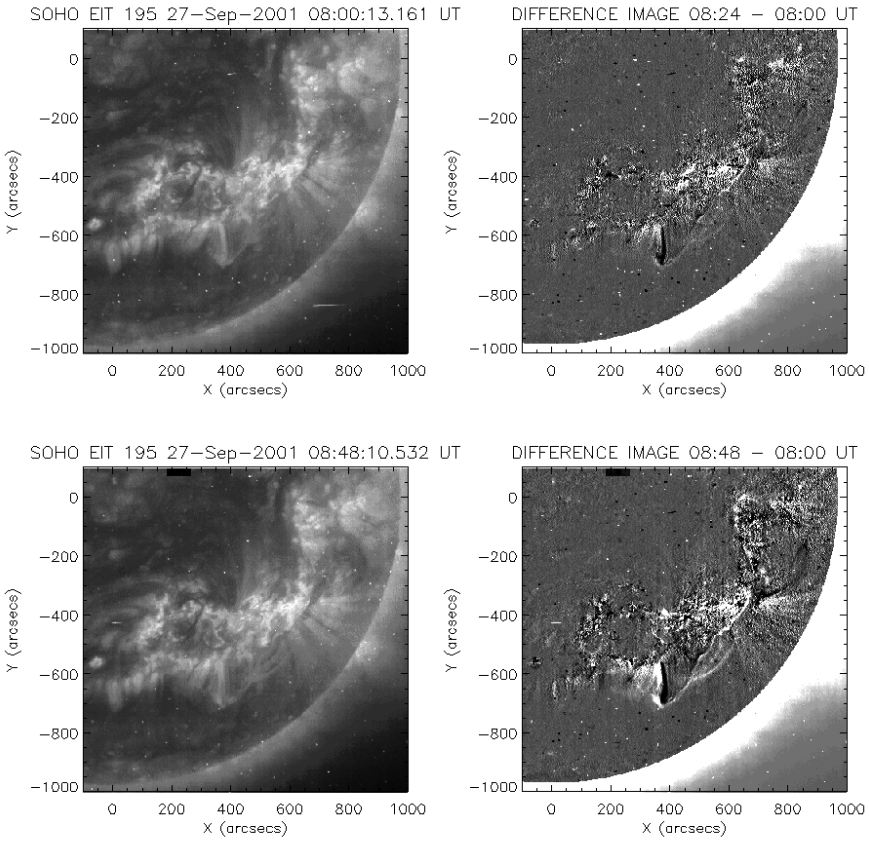

Figure 2. SOHO EIT images at 08:00 and 08:48 UT (on the left) and the base difference images at 08:24 and 08:48 UT (on the right, with base image at 08:00 UT).

would have been located behind the solar limb in the southern hemisphere on the date of our events.

The low X-ray intensity also suggests that not much heated plasma was present within the flaring region, at low heights. CME acceleration without intense flaring occurring in the same time period suggests that reconnection might have taken place high in the corona, thus not showing typical flare signatures.

2.2. Coronal Mass Ejections

Three successive partial halo CMEs were observed to originate from AR 9628 on 27 September 2001. The first CME (CME1) had a typical CME structure with a bright front followed by a cavity and a bright core. It was first observed in the field of view of the SOHO/LASCO C2 coronagraph at 01:32 UT at a projected height 3.35 $R_{\odot}$ directed toward the south in the plane of the sky. The leading-front central position angle calculated counter-clockwise from the north is given as 208 degrees in the LASCO CME catalog. We measured the CME1

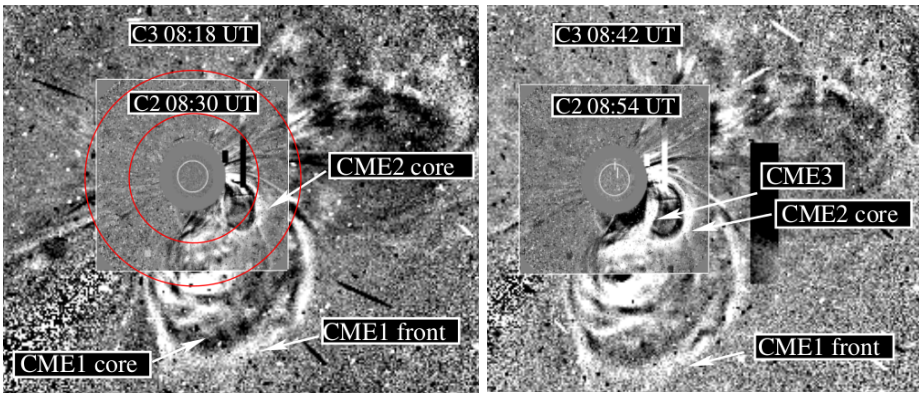

Figure 3. Left: Image composite with LASCO C2 difference image at 08:30 UT and C3 difference image at 08:18 UT, during the time of the first radio type II burst enhancement. The red circles indicate the heights of 4.3 $R_\odot$ (radio source height using Leblanc model densities) and 7.3 $R_\odot$ (hybrid model densities). Right: Image composite with LASCO C2 difference image at 08:54 UT and C3 difference image at 08:42 UT, just after the first radio type II burst had disappeared from the radio spectrum.

leading front heights as a function of time at a position angle 212 degrees, and the CME was visible up to a height of ≈16 $R_\odot$.

The initial speed of CME1 was about 160 km s^{-1}, but after a steady acceleration, it reached a speed of 420 km s^{-1} at the height last observed. We also measured the projected heights of the CME1 core as function of time at the position angle 200 degrees. The first measurement was done at 02:06 UT at height 2.8 $R_\odot$. The core was followed up to ≈30 $R_\odot$ (at 14:42 UT). However, already at 10:20 UT the CME1 core and the core of CME2 (see below) had partly merged together forming a bright front surrounding (in the plane of the sky) the third, faster CME apparently pushing forward the previous two. The initial speed of the CME1 core was well below 100 km s^{-1}, but like the leading front, the core was also accelerating and reached a speed of ≈350 km s^{-1} by ≈09:40 UT, when it suddenly experienced a much stronger acceleration and reached its final speed of 930 km s^{-1} at 14:42 UT.

We have the first measurement of CME2 at 05:06 UT at a projected height of 3.1 $R_\odot$ at the position angle 243 degrees propagating roughly toward the south-west. Like CME1, this CME also had a leading front followed by a core. The leading front was only weakly visible and disappeared already at a height 5.6 $R_\odot$ at 06:54 UT. We followed the CME2 core at the position angle 237 degrees from the height of 3.3 $R_\odot$ at 05:54 UT up to the height of 31.3 $R_\odot$ at 15:42 UT. The initial speed of CME2 core was about 150 km s^{-1}, and it was slowly decelerating. By 08:06 UT its speed had decreased to 130 km s^{-1}, when it suddenly experienced a very strong acceleration and reached the speed of ≈700 km s^{-1} by 09:42 UT at height 8.3 $R_\odot$. By this time, the CME2 core structure had started to merge together with the CME1 core forming the brighter part of the common structure. Its final speed at 15:42 UT was 800 km s^{-1}.

CME3 was first seen in the field of view of the SOHO/LASCO C2 coronagraph at 08:06 UT. We measured the projected heights of CME3 at position angle 212

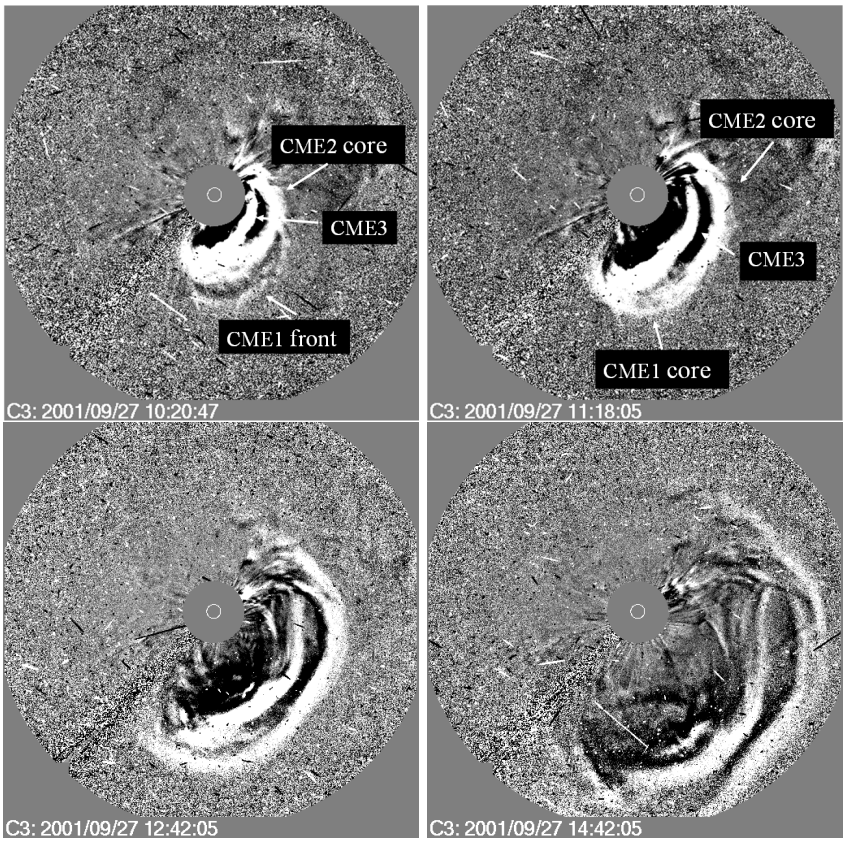

Figure 4. LASCO C3 difference images at 10:20 UT (the last image with visible CME1 front), 11:18 UT, 12:42 UT, and 14:42 UT.

degrees, *i.e.,* the same angle as the leading front of CME1. Our first measurement is at 08:54 UT at height 4.1 $R_{\odot}$. CME3 was initially clearly the fastest of the three with the initial speed of 500 km s^{-1}. It was steadily accelerating, and its final speed was slightly higher (980 km s^{-1}) than that of the two previous CMEs.

The LASCO difference images at selected times are shown in Figures 3 and 4.

2.3. Radio Type II Bursts and their Height Estimates

In the decimeter-meter ranges the dynamic spectra did not contain any metric type II events (HiRAS observations at 25 MHz – 2.5 GHz, Artemis-IV observations at 110 – 500 MHz, DAM data at 20 – 70 MHz). Intense, frequency-drifting type III storm activity was observed during the whole day at frequencies below 100 MHz.

The *Wind*/WAVES experiment observed IP type II bursts after the third flare-CME event, showing plasma emission at the fundamental (F) and harmonic (H) frequencies. The first burst appeared in the spectrum at 08:22 UT and its F-lane emission was spread within the frequency range of 2.40 – 1.45 MHz. Before

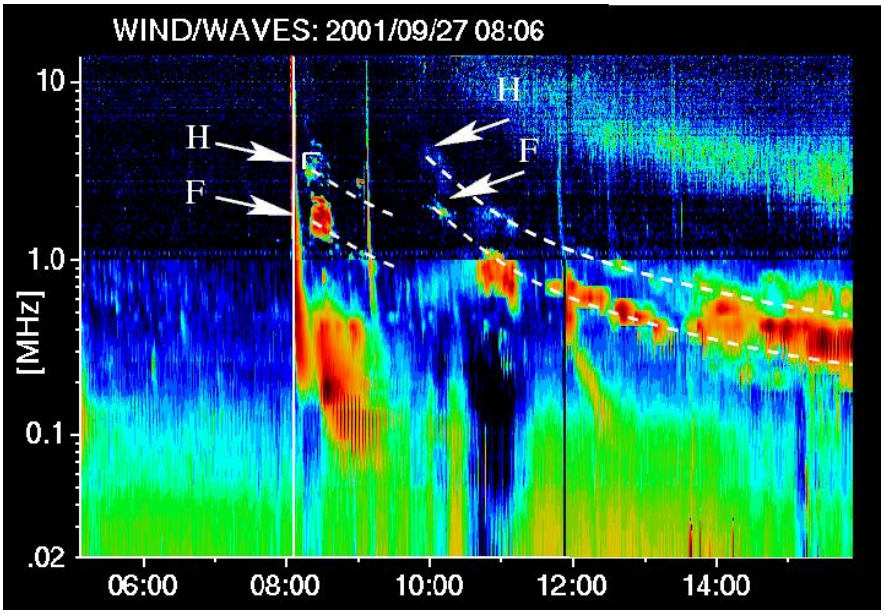

Figure 5. *Wind*/WAVES dynamic spectrum at 05:00 – 16:00 UT on 27 September 2001 showing the frequency range 14 MHz – 20 kHz. The fundamental (F) and harmonic (H) bands of the type II emissions are marked with arrows and the emission lanes are sketched with dashed white lines. The spectral plots are from the CDAW LASCO CME Catalog.

17:30 UT several separate periods of type II emission were recorded, the most intense ones appearing at 08:22 – 08:40 UT, 10:40 – 11:15 UT, 11:50 – 13:25 UT, and 14:00 – 17:20 UT. On closer inspection, the start of the second type II burst (F-lane) was identified near 2 MHz at 10:04 UT. The fundamental (F) and harmonic (H) lanes, judged by eye from the dynamic spectrum, are sketched in Figure 5 by the dashed white lines. The characteristics of the type II burst intervals are listed in Table 2. The type II frequencies given in Table 2 are, however, the lane centres obtained as the peak frequencies of Gaussian fits. Instantaneous relative bandwidths were calculated by dividing the full-widths at half-maximum (FWHM) by the peak frequency at the corresponding time. The FWHM can be interpreted as the error margin, as it presents the difference between the upper and lower lane parts. For the burst starting at 10:04 UT it was not always possible to determine the bandwidth due to the low intensities. The average value of the ratio, which reflects the inhomogeneity of the medium traversed by the shock, is given in Table 2.

In estimating the heights of the type II burst drivers, an atmospheric density model has to be selected. The atmospheric electron density model by Vršnak, Magdalenič, and Zlobec (2004), hereafter called the hybrid density model, merges the high-density low-corona models to the low-density IP models without breaks or discrepancies. The hybrid density model is basically a mixture of the five-fold Saito (1970) model and the model of Leblanc, Dulk, and Bougeret (1998), hereafter called the Leblanc model, with small modifications. The height differences in different atmospheric conditions are presented, for example, in Figure 1 of

Pohjolainen *et al.* (2007). We list heights obtained using both the hybrid and the Leblanc models, as they give the most realistic range of values.

The IP type II bursts and their estimated starting heights and the projected CME heights at the same times are listed in Table 3. The type II burst speeds, estimated using both density models, are also listed in Table 2. The estimated heights of the CME leading fronts and cores and the calculated radio source heights obtained by using both the hybrid and Leblanc models are presented in Figure 6 as function of time. The error bars of the radio heights represent the FWHM bandwidths of the radio emission.

Table 2. Radio type II burst characteristics on 27 September 2001.

Burst (UT)	Lane center[1] (kHz)	FWHM/ peak freq. ratio[2]	Drift rate[3] (kHz s^{-1})	Burst speed[4] (km s^{-1})	Burst speed[5] (km s^{-1})
08:22 – 08:40	1875 – 1730	0.15	0.13	125	200
10:04 – 11:00	2057 – 1000	–	0.31	455	690
10:40 – 11:15	887 – 732	0.23	0.07	360	430
11:50 – 13:25	732 – 387	0.18	0.06	720	745
14:00 – 17:20	542 – 257	0.27	0.02	590	570

[1]Peak position from Gaussian fit, at start and end of burst.
[2] Average value of the instantaneous relative bandwidth obtained from Gaussian fits along the burst lanes.
[3]Linear fit.
[4]Calculated using the Leblanc atmospheric density model.
[5]Calculated using the hybrid atmospheric density model.

Table 3. Radio type II burst heights at the start of emission, calculated using the emission lane center and the hybrid and Leblanc atmospheric density models. Corresponding CME heights, observed in projection, at the same time are given, interpolated between the observed heights if not observed at the same time.

Time (UT)	Lane center (kHz)	Radio height[1] ($R_\odot$)	Radio height[2] ($R_\odot$)	CME1 front height ($R_\odot$)	CME1 core height ($R_\odot$)	CME2 core height ($R_\odot$)	CME3 height ($R_\odot$)
08:22	1875	4.3 ± 0.4	7.3 ± 0.7	12.0	9.1	5.2	< 4.2
10:04	2057	4.1 ± 0.2	6.9 ± 0.4	14.8	12.2	9.4	7.0
10:40	887	6.8 ± 0.6	11.0 ± 1.0	15.9	14.0	11.5	8.8
11:50	732	7.9 ± 0.6	12.3 ± 0.6	–	18.5	15.9	12.8
14:00	542	10.2 ± 0.8	14.8 ± 0.7	–	27.7	24.3	21.3

[1]Leblanc atmospheric density model (normalized to n_e at 1 AU = 7.2 cm^{-3}).
[2]Hybrid atmospheric density model.

3. Formation and Propagation of Coronal Shocks

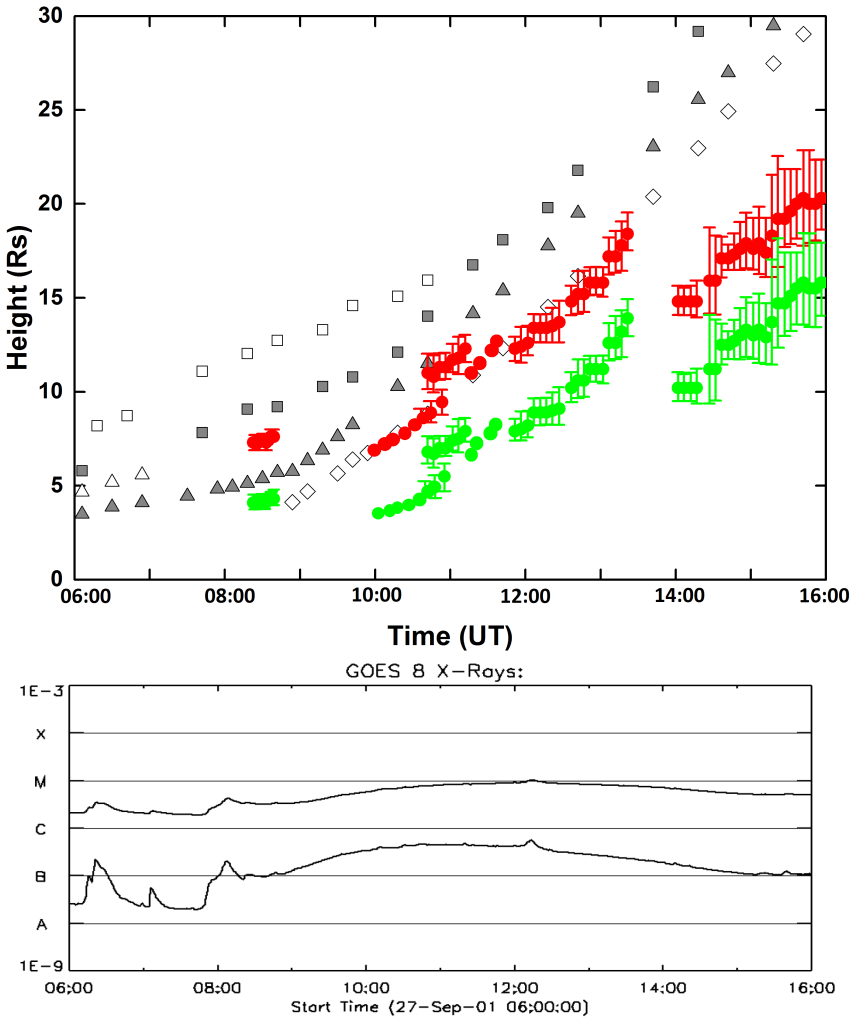

Figure 6. Top: Projected CME leading front heights for CME1 (*squares*), CME2 (*triangles*), and CME3 (*diamonds*). The filled squares and triangles represent the core heights of CME1 and CME2 respectively. The radio source heights were obtained by using the hybrid model (*red circles*) and Leblanc model (*green circles*). The error bars are the FWHM bandwidths of the type II radio emission. Bottom: GOES soft X-ray flux from the full solar disk.

3.1. First IP Type II Burst and Shock

The first IP type II burst appeared at 08:22 UT and the emission covered the frequencies 2.40 – 1.45 MHz. There is indication of band-splitting within the emission lane, and we identified at least three different bands within the emission

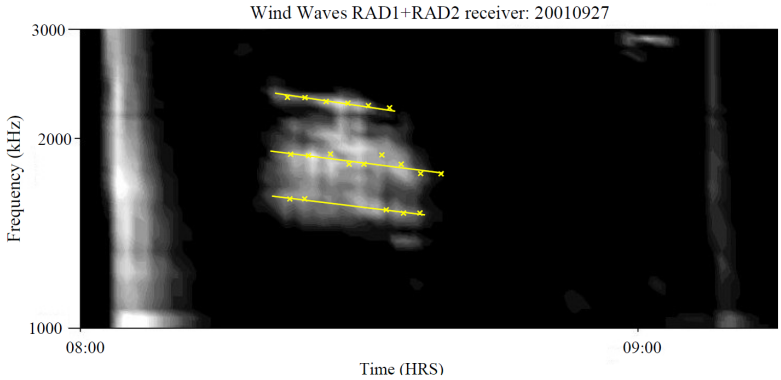

Figure 7. *Wind*/WAVES dynamic spectrum on 27 September 2001 showing band-splits within the first type II burst. The lines indicate bands that were determined by Gaussian fits, but there are structures within the band that could not be reliably identified with this method.

lane, as shown in Figure 7. However, as the center part of the emission lane looks to contain more than one structure, and these structures seem to have different drift rates, the splitting cannot be determined accurately.

The emission peak frequency of the center lane was 1.875 MHz at 08:22 UT near the start of the burst, which corresponds to a density of 4.3×10^4 cm^{-3}. The frequency of 1.875 MHz gives heights of 7.3 $R_\odot$ (hybrid atmospheric density model) and 4.3 $R_\odot$ (Leblanc density model). In Figure 6 the error bars for the heights are the FWHM bandwidths, *i.e.* showing the difference in height if it was calculated using the upper and lower parts of the emission lane. For some time periods it was not possible to determine the peak frequencies or bandwidths from Gaussian fits due to low intensities. The frequencies for these periods were measured along the white dashed line (F) in Figure 5 and are presented in Figure 6 without error bars.

In general, the Leblanc model gives densities that are very low for the active region corona but work well at larger distances, while the hybrid model can be used for connecting bursts that start in the low corona and continue to larger distances in the IP space.

Both models give an electron density of 7.2 cm^{-3} near 1 AU. Of these models, the height given by the Leblanc model is near the heights of the projected CME2 core and the CME3 leading front, see Figure 6.

At 08:37 UT, near the end of the enhanced emission, the peak frequency was 1.73 MHz, which gives a low burst speed from the frequency drift and suggests that the shock was not propagating along the large density gradient (see Table 2). The continuation of the type II burst lane is uncertain after this time, as faint emission features appear in different parts of the spectrum and no obvious continuation can be identified. The CME locations during the first radio burst are shown in the LASCO difference images in Figure 3.

A CME leading front is usually an ejected (dense) loop, a cavity behind the front is a (low-density) filament channel, and the core is a (high-density) erupting filament. CME1 was observed to have these typical structures. The

CME1 core was located some distance away from the radio source, at larger height, as indicated in Figure 3 (where the red circles give the range of the radio source height, as calculated from the two atmospheric models, at 4.3 to 7.3 $R_\odot$, and the CME1 core at the height 9.1 $R_\odot$).

We estimated that the speed of the CME1 core at 08:18 – 08:40 was 300 – 310 km s^{-1}, which is quite slow to be able to drive a shock wave. However, at heights near 8 $R_\odot$ the local Alfvén speed in a standard atmosphere can be as low as 200 km s^{-1} (Vršnak, Magdalenič, and Zlobec, 2004), which would make shock formation possible. In this case the front of the CME1 core would have to be propagating within the low-density cavity. CME cavities have been estimated to have electron depletions of 25% – 50% of the mean coronal densities (Marque, 2004), but in such low densities the local Alfvén speed would also increase, making it difficult for the shock to form and propagate.

As coronal holes were present near the AR, we also calculated possible radio emission heights using coronal hole density values from Fisher and Guhathakurta (1995). The obtained source heights were very low, falling even below the CME3 heights.

At the time of the first type II burst, both the CME1 leading front and the CME1 core were accelerating. While the CME1 leading front was estimated to have a constant acceleration, the CME1 core experienced a sudden increase in acceleration. Due to the uncertainties in identifying the core structures in between the LASCO C2 and C3 fields-of-view, the start time of the faster acceleration of the core cannot be determined accurately, but the best fit of our height-time measurements indicates a significant velocity change near the time of the first observation of CME3 and the appearance of the second type II burst, see Figure 6. The first radio burst disappeared from the dynamic spectrum at 08:40 UT, with no obvious changes in the observed features at heights 7 – 8 $R_\odot$ (Figure 3).

3.2. Second IP Type II Burst and Shock

The second type II burst appeared at 10:04 UT at ≈2 MHz. This emission was relatively faint and had a narrow bandwidth. After about 10:20 UT there also appears a relatively diffuse feature, possibly a type III storm, drifting down from about 10 MHz to lower frequencies during the day.

Three periods of more enhanced emission occurred after 10:40 UT. The first two enhanced emission lanes look to have similar drift rates. The third enhancement occurred at slightly higher frequencies and had a larger bandwidth (see Figure 5). This suggests that the emission driver could have been the same shock, with the third burst part occurring in a slightly denser plasma environment (see Figure 6 for the estimated heights). The emission at 10:40 – 11:15 UT was quite broad-band and it is also possible that the low-frequency part of it is connected to the first type II burst starting at 08:22 UT, if the burst emission drifted along the dashed line shown in Figure 5.

For the start of the second shock, the radio source heights calculated with the hybrid model suggest that the shock was formed near the leading front of CME3. The heights given by the Leblanc model fall behind all the CME leading front heights, suggesting a shock near the CME flanks.

The last part of type II emission started at 14:00 UT and the emission lane was observed to spread to higher frequencies, covering the frequency range between the F and H lanes. Similar-looking "splashes" of emission have been interpreted as a radio signature of the CME – CME interaction (Gopalswamy *et al.*, 2001). As higher frequencies mean higher densities, we interpret that the spread was caused by the propagating shock meeting higher-density material. Hence, the heights shown in Figure 6 may be too low, as well as the obtained shock velocity of 570 km s^{-1} (hybrid density model). The LASCO C3 image at 14:42 UT (Figure 4) shows how the overall structure of the CMEs remained the same, but that some merging of the CMEs occurred.

3.3. Shock Arrival near Earth

Shock arrival near Earth was reported by Reiner, Kaiser, and Bougeret (2007) at 09:29 UT on 29 September, with a shock arrival speed of 611 km s^{-1}. They list that the associated flare/CME was the last of the three, CME3. The ICME list[1] gives the shock arrival time as 09:27 UT, with an ICME arrival at 14:17 UT, on 29 September. Another shock arrival is reported at 19:13 UT, with an ICME arrival at 22:48 UT, on 30 September. Also the *Harvard-Smithsonian Center For Astrophysics* (CfA) Interplanetary Shock Database[2] lists these two shocks. The SOHO CELIAS/PM shock list[3] reports two shocks at comparable times, but does not, however, connect these shocks to any source origins.

The transit time of the first shock, from 12:00 UT on 27 September (13.4 $R_\odot$) to 09:00 UT on 29 September (L1 at 212.8 $R_\odot$) would be 45 hours, and the average transit velocity would then be ≈860 km s^{-1}. This means that the shock would have had to accelerate from the estimated velocities near the Sun, and then slow down to the observed 611 km s^{-1} near Earth.

The second shock, arriving on 30 September at 19:13 UT, would have had a transit time of 79 hours 13 min and average transit velocity of ≈490 km s^{-1}. As on 28 September two fast CMEs occurred, one halo and one partial-halo (first observed at 08:54 UT with a linear fit speed 846 km s^{-1}, and at 10:30 UT with a linear fit speed 665 km s^{-1}), and the WAVES spectrum shows a wide type II-like emission lane after these events, it is more probable that the arrival of the second shock was related to one of these later CMEs.

The type II burst emission lane that started on 27 September was identifiable in the dynamic spectrum only until the early hours of 28 September, so observationally no direct connection to the arriving shocks can be made.

4. Discussion

Our analysis has presented several questions concerning the formation of the first type II burst, which occurred at low frequencies (*i.e.* in a low density region).

[1]See http://space.ustc.edu.cn/dreams/wind_icmes/.

[2]See https://www.cfa.harvard.edu/shocks/wi_data/wi_2001.html.

[3]See http://www.mssl.ucl.ac.uk/~rdb/helio-hec/out/soho_pm_shock.html.

If the height of the first type II burst calculated from the hybrid atmospheric density model (7.3 $R_\odot$) is true, then why does the shock start so high in the atmosphere and what is the shock driver, when no high-speed CME features are observed near the radio source height?

One possibility would be a back-side event, where a type II burst would become visible after reaching a projected height above the solar limb. But, in this event we could not identify any active region that could have been the source of a shock wave propagating on the backside of the Sun. Another possibility is, however, that the shock wave did propagate from the low corona, but there the conditions for the generation of radio emission were not favourable, and hence we did not observe associated type II radio emission. The sudden acceleration of the CME2 core and continuous acceleration of CME1 and CME3 were observed at the time of the first radio burst, but the CME2 core and CME3 leading front (observed in projection) were located at much lower heights, near $4-5$ $R_\odot$, and the CME1 core was at a much larger height, near 9 $R_\odot$. A height difference of $\approx$2 $R_\odot$ corresponds to about 1.4 million km, and a "push" of the accelerating CMEs could not have travelled that far within the time period between the start of CME acceleration and the appearance of the first radio burst.

The Leblanc density model (Leblanc, Dulk, and Bougeret, 1998) gives a radio source height (4.3 $R_\odot$) for the first type II burst that is very close to the CME2 core and CME3 leading front heights, but this density model gives far too low radio heights for later type II burst parts. Here we also have to take into account the errors in estimating CME heights and speeds, as they are observed in projection on the plane of the sky. But, as type II bursts do not suffer from projection effects, their height-time propagation can be used for comparison. We also note the large uncertainty in radio burst heights, caused by the selection of an atmospheric density model. The second type II burst looks to originate either as a bow shock near the leading front of CME3, or at lower heights near the CME flanks if a low-density atmospheric model is applied. A low-density corona could be possible in the wake of the three CMEs, as they would have depleted a large part of the coronal plasma. Whether the shock could have occurred in the flanks of CME2 or CME3 cannot be determined, as these structures had very similar projected heights.

5. Conclusions and Summary

There are many possibilities for the formation of the type II bursts but the following suggestions get support from our data analysis:

The first radio type II burst could be due to a shock wave launched by sudden acceleration of the CME2 core and accelerating CME3 if the plasma densities were very low ahead of the CMEs, or by accelerating CME1 core if the plasma densities were very high inside the CME1 cavity. The shock may have been propagating sideways. It showed a frequency drift that indicates low speed, but only if the shock was propagating radially outwards. In the case of non-radial propagation the density decrease is slower allowing a higher propagation speed with the derived frequency drift. The low-density environment of the first type

II shock suggests that some sort of density depletion was present in the shock-forming region, although it could not be identified in the images. The decrease of the intensity of the type II harmonic band at lower frequencies is most probably due to the fact that plasma conditions in the interplanetary space favour the appearance of the fundamental plasma emission band, instead of the harmonic band (the opposite happens in the corona at higher frequencies). Shocks may also stop if, for example, the Alfvén speed rises rapidly. The uncertain continuation of the fundamental band below ≈1 MHz may reflect a change in the local plasma conditions.

The start of the second type II burst at higher frequencies indicates that it was due to a separate shock, propagating to a different direction, within different atmospheric density. The second radio burst appeared near the time when the CME1 core started propagating faster, pushed by CME3. Our estimates of the radio source heights suggest that it could also have been a shock at the flanks of either CME2 or CME3.

As the CME3 heights were approaching the heights of CME2 (both observed in projection), CME – CME interaction was most probably present and hence the type II emission showed an increased frequency range in the later stages of emission. Sporadic enhancements can be caused by irregularities in the solar wind, like plasma from the earlier transients, as in Knock *et al.* (2003).

Only one shock that could reliably be related to the investigated CMEs was observed to arrive near Earth. This suggests that before reaching the near-Earth space, all the CMEs had merged together and only the shock that was created ahead of this merged structure continued to propagate near Earth.

Acknowledgments We are grateful to the anonymous referee, whose comments and suggestions greatly improved this article. This work was supported by the grant 4438/2013 from the Ministry of Higher Education and Scientific Research of Iraq. We are grateful to all the individuals who have contributed in creating and updating the various solar event catalogues. The SOHO/LASCO CME Catalog is generated and maintained at the CDAW Data Center by NASA and the Catholic University of America in cooperation with the Naval Research Laboratory. The *Wind*/WAVES radio type II burst catalog has been prepared by Michael L. Kaiser and is maintained at the Goddard Space Flight Center. SOHO is a project of international cooperation between ESA and NASA.

Disclosure of Potential Conflicts of Interest The authors declare that they have no conflicts of interest.

References

Bougeret, J.-L., Kaiser, M. L., Kellogg, P. J., Manning, R., Goetz, K., Monson, S. J., Monge, N., Friel, L., Meetre, C. A., Perche, C., Sitruk, L., Hoang, S.: 1995, *Space Sci. Rev.* **71**, 231. DOI 10.1007/BF00751331

Brueckner, G. E., Howard, R. A., Koomen, M. J., Korendyke, C. M., Michels, D. J., Moses, J. D., Socker, D. G., Dere, K. P., Lamy, P. L., Llebaria, A., Bout, M. V., Schwenn, R., Simnett, G. M., Bedford, D. K., Eyles, C. J.: 1995, *Solar Phys.* **162**, 357. DOI 10.1007/BF00733434

Cane, H. V., Erickson, W. C.: 2005, *Astrophys. J.* **623**, 1180. DOI 10.1086/428820

Cho, K.-S., Moon, Y.-J., Dryer, M., Shanmugaraju, A., Fry, C. D., Kim, Y.-H., Bong, S.-C., Park, Y.-D.: 2005, *J. Geophys. Res.* **110**, A12101. DOI 10.1029/2004JA010744

Cliver, E. W., Webb, D. F., Howard, R. A.: 1999, *Solar Phys.* **187**, 89. DOI 10.1023/A:1005115119661

Delaboudinière, J.-P., Artzner, G.E., Brunaud, J., Gabriel, A.H., Hochedez, J.F., Millier, F., Song, X. Y., Au, B., Dere, K. P., Howard, R. A., Kreplin, R., Michels, D. J., Moses, J. D., Defise, J. M., Jamar, C., Rochus, P., Chauvineau, J. P., Marioge, J. P., Catura, R. C., Lemen, J. R., Shing, L., Stern, R. A., Gurman, J. B., Neupert, W. M., Maucherat, A., Clette, F., Cugnon, P., van Dessel, E. L.: 1995, *Solar Phys.* **162**, 291. DOI 10.1007/BF00733432

Dryer, M.: 1996, *Solar Phys.* **169**, 421. DOI 10.1007/BF00190618

Fisher, R., Guhathakurta, M.: 1995, *Astrophys. J.* **447**, L139. DOI 10.1086/309582

Gopalswamy, N., Kaiser, M. L., Lepping, R. P., Kahler, S. W., Ogilvie, K., Berdichevsky, D., Kondo, T., Isobe, T., Akioka, M.: 1998, *J. Geophys. Res.* **103**, 307. DOI 10.1029/97JA02634

Gopalswamy, N., Yashiro, S., Kaiser, M. L., Howard, R. A., Bougeret, J.-L.: 2001, *Astrophys. J. Lett.* **548**, L91. DOI 10.1086/318939

Gopalswamy, N., Yashiro, S., Kaiser, M. L., Howard, R. A., Bougeret, J.-L.: 2002, *Geophys. Res. Lett.* **29**, 1265. DOI 10.1029/2001GL013606

Gopalswamy, N., guilar-Rodriguez, E., Yashiro, S., Nunes, S., Kaiser, M. L., Howard, R. A.: 2005, *J. Geophys. Res.* **110**, A12s07. DOI 10.1029/2005JA011158

Gosling, J. T.: 1993, *J. Geophys. Res.* **98**, 18937. DOI 10.1029/93JA01896

Knock, S. A., Cairns, I. H.: 2005, *J. Geophys. Res.* **110**, A01101. DOI 10.1029/2004JA010452

Knock, S. A., Cairns, I. H., Robinson, P. A., Kuncic, Z.: 2003, *J. Geophys. Res.* **108**, 1126. DOI 10.1029/2002JA009508

Lara, A., Gopalswamy, N., Nunes, S., Muñoz, G., Yashiro, S.: 2003, *Geophys. Res. Lett.* **30**, 8016. DIO 10.1029/2002GL016481

Leblanc, Y., Dulk, G.A., Bougeret, J-L.: 1998, *Solar Phys.* **183**, 165. DOI 10.1023/A:1005049730506

Maričić, D., Vršnak, B., Dumbović, M., Žic, T., Roša, D., Hržina, D., Lulić, S., Romštajn, I., Bušić, I., Salamon, K., Temmer, M., Rollett, T., Veronig, A., Bostanjyan, N., Chilingarian, A., Mailyan, B., Arakelyan, K., Hovhannisyan, A., Mujić, N.: 2014, *Solar Phys.* **289**, 351. DOI 10.1007/s11207-013-0314-8

Marqué, C.: 2004, *Astrophys. J.* **602**, 1037. DOI 10.1086/381085

Pohjolainen, S., Allawi, H., Valtonen, E.: 2013, *Astron. Astrophys.* **558**, A7. DOI 10.1051/0004-6361/201220688

Pohjolainen, S., van Driel-Gesztelyi, L., Culhane, J. L., Manoharan, P. K., Elliott, H. A.: 2007, *Solar Phys.* **244**, 167. DOI 10.1007/s11207-007-9006-6

Prakash, O., Umapathy, S., Shanmugaraju, A., Vršnak, B.: 2009, *Solar Phys.* **258**, 105. DOI 10.1007/s11207-009-9396-8

Reiner, M. J., Kaiser, M. L., Bougeret, J-L.: 2007, *Astrophys. J.* **663**, 1369. DOI 10.1086/518683

Robbrecht, E. Patsourakos, S. Vourlidas, A.: 2009, *Astrophys. J.* **701**, 283. DOI 10.1088/0004-637X/701/1/283

Saito, K.: 1970, *Ann. Tokyo Astr. Obs.* **12**, 53. (no DOI)

Shanmugaraju, A., Moon, Y.-J., Dryer, M., Umapathy, S.: 2003, *Solar Phys.* **215**, 185. DOI 10.1023/A:1024808819850

Smerd, S. F. Sheridan, K. V. Stewart, R. T.: 1974, In: Newkirk, G.A. (ed.) *Coronal Disturbances*, IAU Symp. **57**, Reidel, Dordrecht, 389.

Smerd, S. F. Sheridan, K. V. Stewart, R. T.: 1975, *Astrophys. Lett.* **16**, 23

Treumann , R. A. Labelle , J.: 1992, *Astrophys. J. Lett.* **399**, L167. DOI 10.1086/186633

Tsuneta, S., Acton, L., Bruner, M., Lemen, J., Brown, W., Caravalho, R., Catura, R., Freeland, S., Jurcevich, B., Morrison, M., Ogawara, Y., Hirayama, T., Owens, J.: 1991, *Solar Phys.* **136**, 37. DOI 10.1007/BF00151694

Vršnak, B., Magdalenič, J., Zlobec, P.: 2004, *Astron. Astrophys.* **413**, 753. DOI 10.1051/0004-6361:20034060